Revisiting Waal River Training by Historical Reconstruction

Le, T.B.; Crosato, A.; Montes Arboleda, A.

DOI
10.1061/(ASCE)HY.1943-7900.0001688

Publication date
2020

Document Version
Final published version

Published in
Journal of Hydraulic Engineering

Citation (APA)
Le, T. B., Crosato, A., & Montes Arboleda, A. (2020). Revisiting Waal River Training by Historical Reconstruction. *Journal of Hydraulic Engineering*, *146*(5), 05020002-1 - 05020002-14. Article 05020002. https://doi.org/10.1061/(ASCE)HY.1943-7900.0001688

Case Study

Revisiting Waal River Training by Historical Reconstruction

T. B. Le, Ph.D.[1]; A. Crosato[2]; and A. Montes Arboleda[3]

Abstract: The Dutch River Waal, a branch of the Rhine, has been trained for centuries to mitigate the effects of ice-jams and improve navigation. The works, started in 1850, involved river straightening and narrowing by a series of transverse groynes. Besides fulfilling their goal, the groynes also created the need to raise flood protection works and caused undesirable channel incision. This study assesses the effectiveness of training the river with a longitudinal wall instead of with groynes. The investigation analyzes the long-term response of the historical river with a two-dimensional depth-averaged (2DH) morphodynamic model. The results show that the wall would create two parallel channels, one becoming deeper and the other one shallower. The former would be as suitable for navigation as an equally-wide channel obtained with groynes. The latter would contribute in conveying water during high flow events and improve the river ecology. Training the river with a wall would also lessen channel incision. The best performance is obtained if the wall is built on the channel centerline, starting just upstream of a point bar top. **DOI: 10.1061/(ASCE)HY.1943-7900.0001688.**

Author keywords: Historical Waal river; River training; Longitudinal training wall; Groynes; River morphology; Navigation; Flood conveyance; Delft3D.

Introduction

Background Information

The frequency of dike breaches and flooding increased along the Waal River, a branch of the Rhine, in the early modern period. At least 29 out of 51 river dike breaches between 1757 and 1926 were provoked by ice jams (Wijbenga et al. 1993, 1994). As these ice jams formed preferentially at wider shallow sections with bars and islands, it was decided to give the river a narrow uniform width using a series of transverse groynes. For this, since 1850, the width of the Waal River was reduced to 360 m, 310 m, and finally to 260 m. To improve navigability, in the second decade of the twentieth century, the river was also straightened and dredged. Fig. 1 shows the different phases of the river training program, called *Normalization*.

The morphological response of the river to narrowing, straightening, and sediment extraction resulted in an incision process that reached the rate of 2 cm/year (Sieben 2009). Besides floodplain draining and deterioration of riparian habitats, the lowering of the channel bed also posed problems to the hydraulic structures along the river, including the groynes. The conditions for navigation gradually deteriorated because the connection between the river and the other elements of the inland waterway network, such as canals, ship locks, and fluvial port facilities, became problematic. In addition, transverse groynes produce shallow ridges as a response to the formation of scour holes at their heads, which hampers navigation even further (Yossef 2005). Finally, a series of groynes hinders the flow at high discharges, forcing the water level to increase (Huthoff et al. 2013).

In 2013–2015, three series of transverse groynes were replaced by longitudinal training walls near the city of Tiel (the Netherlands), as an attempt to mitigate these effects (Fig. 2). The main idea of this pilot project was to create a narrow and sufficiently deep navigation channel at low flows and a two-channel system to convey water at high flows, reducing the channel incision process and lowering water levels. The new channel behind the training wall, a freely flowing stream without intensive shipping traffic and with a more natural bank, was expected to improve the river ecological conditions. However, the effectiveness of these interventions in achieving the goals has not been thoroughly investigated yet, particularly on the long-term.

Navigation is common in low-land rivers, like the Waal, especially in the final part of their course, close to the sea. The bed of these rivers often presents bars and point bars inside bends. These large sediment deposits are characterized by transverse bed slopes and produce helical flows, with the result that they locally modify the sediment transport direction. The presence of a nearby bar is thus expected to alter the distribution of sediment at the bifurcation created by a longitudinal training wall and hence to influence bifurcation stability (Bertoldi and Tubino 2007). Le et al. (2018a, b) carried out a series of experimental tests as well as numerical simulations showing that the parallel-channel system created by a longitudinal training wall tends to be unstable. The most stable configuration is obtained with equally-wide parallel channels. Both channels remain open, one deeper and one shallower, if the upstream

[1]Faculty of Civil Engineering, Thuyloi Univ., 175 Tay Son, Dong Da, Hanoi 116705, Vietnam; Dept. of Hydraulic Engineering, Faculty of Civil Engineering and Geosciences, Delft Univ. of Technology, P.O. Box 5048, 2600 GA Delft, Netherlands. ORCID: https://orcid.org/0000-0003-2100-4732

[2]Associate Professor of River Morphology and River Engineering, Dept. of Hydraulic Engineering, Faculty of Civil Engineering and Geosciences, Delft Univ. of Technology, P.O. Box 5048, 2600 GA Delft, Netherlands; Dept. of Water Resources and Ecosystems, IHE Delft, P.O. Box 3015, 2601 GA Delft, Netherlands (corresponding author). Email: a.crosato@un-ihe.org

[3]Greeley and Hansen Colombia, Carrera 7#71-21, Oficina 1305, Bogotá 110231, Colombia.

Note. This manuscript was submitted on August 31, 2018; approved on July 11, 2019; published online on March 3, 2020. Discussion period open until August 3, 2020; separate discussions must be submitted for individual papers. This paper is part of the ***Journal of Hydraulic Engineering***, © ASCE, ISSN 0733-9429.

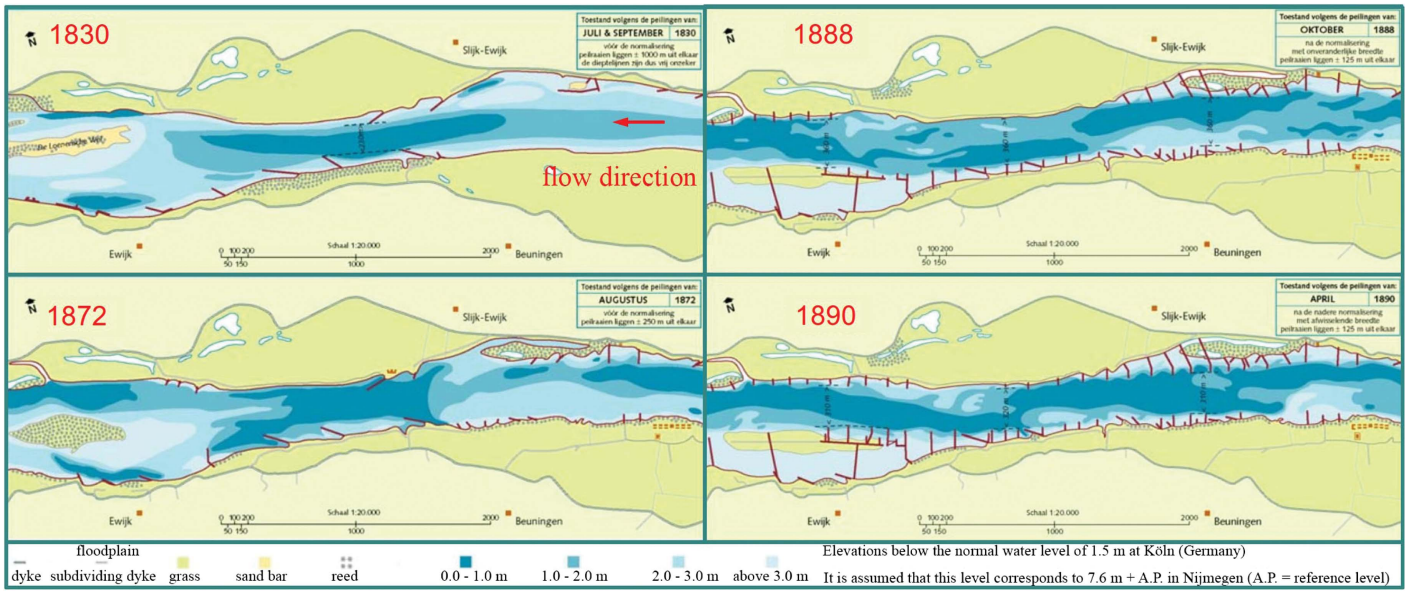

Fig. 1. Normalization of the River Waal by straightening and narrowing by a series of groynes. Red arrow indicates flow direction. (Reprinted from Henket et al. 1885–1890.)

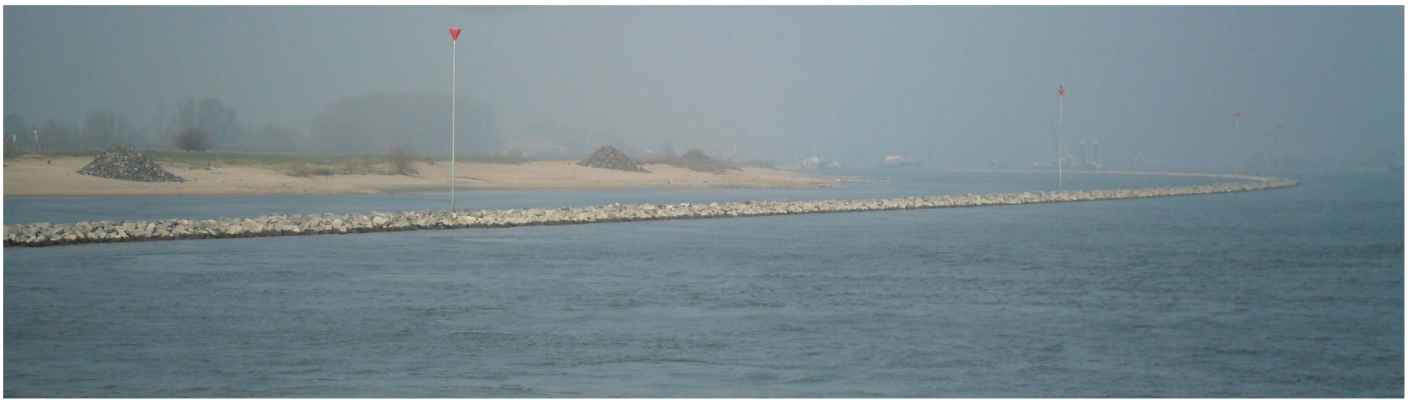

Fig. 2. Longitudinal training wall replacing transverse groynes in the Waal River at Wamel, opposite the city of Tiel, on March 17, 2016. (Image courtesy of Tom Buijse.)

end of the wall is located near the top of a steady alternate-bar or of a point-bar.

This work aims to assess the effectiveness of training the Waal River with a longitudinal training wall instead of groynes with a numerical model, starting from the situation of the river before the *Normalization* works when the river channel was almost twice as wide as now. The large natural width of the historical Waal allows splitting the river in two equally-wide channels, each of them being large enough to potentially become a deep inland water way. The other channel, expected to become much shallower and with a natural bank, seems suitable to eventually host a richer riverine ecosystem than the current groyne fields. For this reason, the channel that becomes deeper is, in this study, termed the *navigation channel* and the one that becomes shallower the *ecological channel*. The effectiveness and convenience of training the river with a longitudinal wall are assessed by comparing the long-term morphological developments obtained with the wall to the ones obtained with series of groynes along both banks and to the *natural* development of the river (untrained case). The focus is on channel incision, channel navigability, and flood conveyance.

The long-term morphological responses are reproduced with a two-dimensional depth-averaged (2DH) model based on the open-source Delft3D code. The numerical approach adopted in this study is supported by Le et al. (2018b), who successfully reproduced the long-term morphological developments observed in an experimental channel separated by a longitudinal training wall; by McCoy et al. (2008), who modeled a channel with a series of groynes; by Arboleda et al. (2010), who simulated floodplain sedimentation in the historical Waal River; and by Vargas-Luna et al. (2018), who successfully applied Baptist et al.'s (2003) formulation, implemented in Delft3D, for the assessment of the effects of floodplain vegetation on water levels.

Study Area

The Waal River is the largest branch of the Rhine in the Netherlands, crossing the country from East to West. The study area is a 12-km long reach of the river located near Slijk-Ewijk, 6 km downstream of the city of Nijmegen (Fig. 3), before the *Normalization* works, when the river was twice as large as it is now (1842 AD—Latin for Anno Domini, which means in the year of the Lord, indicating how many years have passed since the birth of Jesus). The site was selected due to the availability of historical data (Schoor et al. 1999; Arboleda et al. 2010).

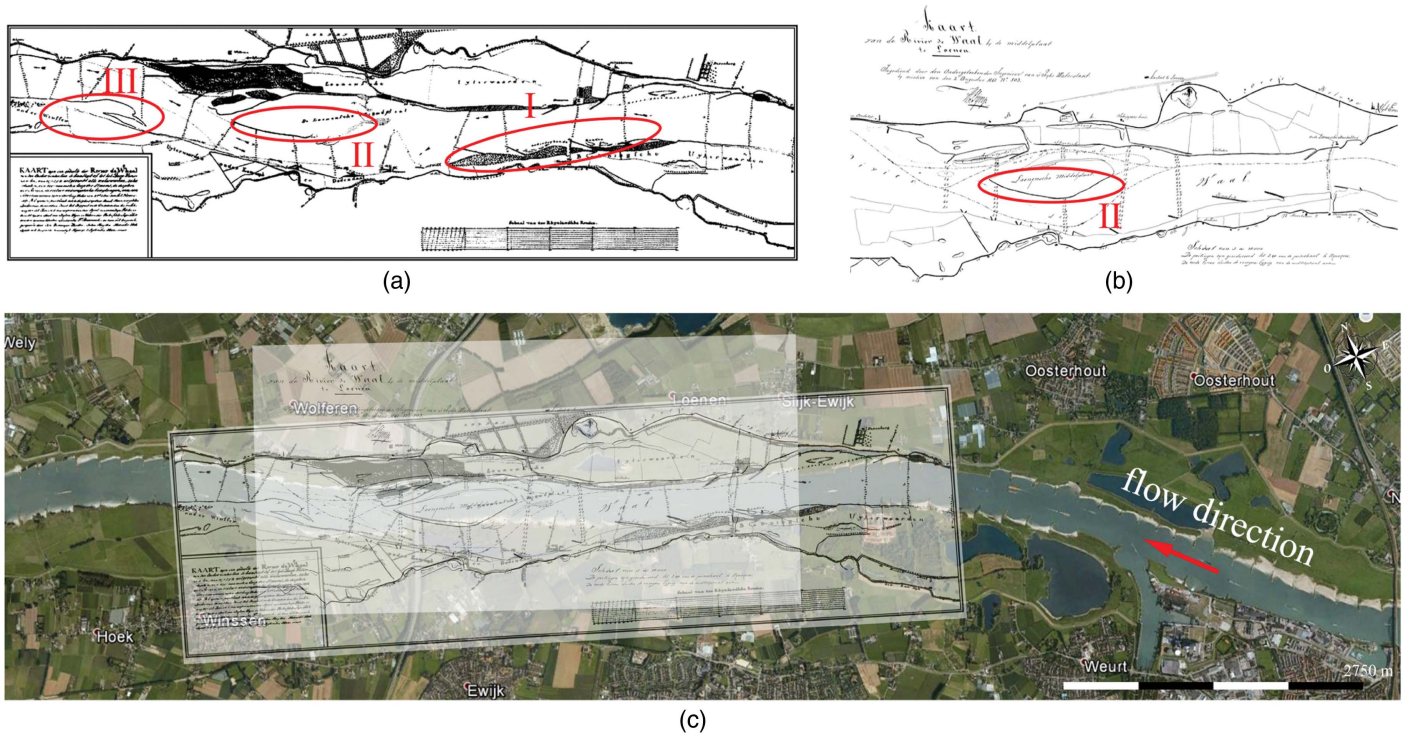

Fig. 3. Study area: Waal River near Slijk-Ewijk, 6 km downstream of the city of Nijmegen: (a) 1800 map; (b) 1842 map; and (c) historical maps superimposed on 2017 Google image. Bars are numbered I, II, and III to be recognized and compared in the calibration and validation steps. [Reprinted (a–c) from Henket et al. 1885–1890; map data for (c) from Google Earth, © 2017 Aerodata International Survey.]

Data on historical bed topographies, converted from local water depths into bed levels relative to the current sea reference level are provided by Rijkswaterstaat (RWS)—Ministry of Infrastructure and Water Management of the Netherlands. An old river map of 1800 AD showing the presence of three bars [Fig. 3(a)] and a set of 17 reconstructed cross-sectional profiles (Maas et al. 1997) allow for model calibration. Another map of the same area in 1842 AD, with five reconstructed cross-sectional profiles [Fig. 3(b)], allows for model validation and provides the start conditions for the simulations of the long-term morphological developments of the river trained either with a longitudinal wall, with groynes, or without any training structures. Both historical maps fit the current situation well, showing their reliability [Fig. 3(c)]. Note that the current river channel alignment is straighter than the original one.

In the study area, the prenormalization channel width was approximately 400 m. By hypothetically dividing it in two equally-wide parts by means of a longitudinal wall, two parallel 200 m wide channels are obtained. This width appears sufficient for navigation, considering that the current river width is 230–260 m.

The historical daily discharge time series were reconstructed by Arboleda et al. (2010) based on the work of van Vuren (2005) and refer to the period 1790–1810. From these time series, the historical daily mean discharge results 1,550 m^3/s, which is rather similar to the current value of 1,490 m^3/s, was obtained from the time series of the period 2000–2010 (M. Schoor, personal communication, 2009–2018). The estimated historical bankfull discharge in the study area is 2,350 m^3/s. The current value is approximately 300 m^3/s higher (it depends on location) due to the channel incision process, which has followed the *Normalization* works.

In the early 1800s, the median grain size of bed material was 850–1,000 μm (Maas et al. 1997), slightly smaller than the present one (Frings and Kleinhans 2008; Frings et al. 2009). Arboleda et al. (2010) showed that suspended solids concentrations were similar to the actual ones, ranging between 85 and 95 mg/L, which is the composition of suspended sediment being silt and fine sand (Middelkoop 1997).

Materials and Methods

General Description

Three wall scenarios are analyzed. In the first two, the longitudinal wall subdivides the river in two equally-wide channels (200 m), as recommended by Le et al. (2018a, b), because this subdivision leads to a rather stable configuration in which both channels tend to remain open. Le et al. (2018b) also showed that starting the wall upstream of, or near to, a point bar top leads to sedimentation in the channel located at the bar side, whereas starting the wall much more downstream, close to or in the subsequent pool, leads to sedimentation in the channel at the opposite side. To cover these two opposite morphological developments, two cases are considered: a wall starting 500 m upstream of point bar I top (Fig. 3) and a wall starting 2,500 m downstream of the same bar top. In the third scenario, the wall, starting 500 m upstream of point bar I top, subdivides the river in two parallel channels with the eroding one having a width equal to the current navigation channel (260 m).

Two groyne-scenarios are considered: (1) a channel width between groynes heads (river-flow width) equal to half of historical Waal River width (200 m); and (2) a channel width between groynes heads equal to the current Waal River width (260 m).

The considered temporal scale corresponds to the time needed to achieve morphodynamic equilibrium in which the long-term temporal changes of two-dimensional (2D) and one-dimensional (1D) bed topography (bar configuration and longitudinal slope) become negligible.

The morphodynamic models used for the investigation are built from Arboleda et al.'s (2010) setup, who reconstructed the historical Waal River using the open-source Delft3D code. However, the present models include some important modifications, as for instance having a mobile bed instead of a fixed bed.

Delft3D solves the Reynolds equations for incompressible fluid and shallow water in three dimensions with a finite-difference scheme (Deltares 2014). The bed level changes are either derived by applying the Exner approach, i.e., by assuming immediate response of the sediment transport rate to the local hydraulic conditions, which is valid only for bed load, or by applying a sediment balance equation in which sediment deposition and entrainment rates are obtained from suspended solids concentrations, hydrodynamic parameters, and soil characteristics. In the Exner approach, the sediment transport rates are computed by means of sediment transport capacity formulas. In the sediment balance approach, the evolution of suspended solids concentration is computed with an advection-diffusion equation. In this study, sediment is assumed to be transported as a bed load. The effects of a transverse slope and spiral flow on the bed load direction are important for the simulation of the evolution of the river bed topography (Mosselman and Le 2016), in particular for the reproduction of bars (e.g., Schuurman et al. 2013), and to simulate the sediment distribution between bifurcating channels (e.g., Kleinhans et al. 2008). For the combined effect of a transverse slope and spiral flow, Struiksma et al. (1985) derived the direction β_s of sediment transport (bed load) as

$$\tan\beta_s = \frac{\sin\beta_\tau - \frac{1}{f(\theta)}\frac{\delta z}{\delta y}}{\cos\beta_\tau - \frac{1}{f(\theta)}\frac{\delta z}{\delta x}} \tag{1}$$

where $\delta z/\delta y$ = transverse slope; $\delta z/\delta x$ = streamwise slope; β_τ = bed shear stress; and $f(\theta)$ = function to account for the effects of the transverse bed slope on the bed load direction in which θ represents the Shields parameter. Considering the effects of spiral flow, which become relevant if the stream lines have a sinuous path, as in channel bends and around bars, the bed shear stress (β_τ) is derived as follows (Struiksma et al. 1985)

$$\tan\beta_\tau = \frac{v}{u} - A\frac{h}{R} \tag{2}$$

where u and v = streamwise and transverse velocity, respectively (m/s); h = local water depth (m); R = streamline radius of curvature (m); and A = coefficient that weights the influence of the spiral flow, derived as follows (Struiksma et al. 1985)

$$A = \frac{2\varepsilon}{\kappa^2}\left(1 - \frac{\sqrt{g}}{\kappa C}\right) \tag{3}$$

with ε ($\approx$1) being a calibration coefficient (in this study $\varepsilon = 1$); κ (=0.4) being the Von Kármán constant; and g and C being the acceleration due to gravity (m/s^2) and the Chézy roughness coefficient (m$^{1/2}$/s), respectively.

The function $f(\theta)$ is derived by applying the formulation suggested by Koch and Flokstra (1981), extended by Talmon et al. (1995)

$$f(\theta) = A_{sh}\theta^{B_{sh}}\left(\frac{D_{50}}{h}\right)^{C_{sh}} \tag{4}$$

where D_{50} = median sediment size; and A_{sh}, B_{sh}, and C_{sh} = calibration coefficients, with A_{sh} being the most sensitive one with a value that normally falls between 0.1 and 1.0. The effects of a transverse slope on the sediment transport direction decrease if the value of A_{sh} increases (Schuurman et al. 2013) and vice versa. In this study, the value of A_{sh} is calibrated, whereas the other coefficients are kept constant with the values suggested by Talmon et al. (1995): $B_{sh} = 0.5$ and $C_{sh} = 0.3$.

In the morphodynamic model, the drying/wetting of cells is obtained based on the local water depth. The cells that become dry are removed from the computational domain and remain dry until higher discharge floods them again. In this study, the threshold value below which cells become dry is 10 cm.

In the presence of vegetation, as for instance on floodplains during high flow events, the Delft3D code corrects the local Chézy coefficient applying Baptist et al.'s (2003) approach

$$C = \frac{1}{\sqrt{\frac{1}{C_b^2} + \frac{C_D n h_v}{2g}}} + \frac{\sqrt{g}}{\kappa}\ln\left(\frac{h}{h_v}\right) \tag{5}$$

where C_b = bed roughness without vegetation (m$^{1/2}$/s); C_D = drag coefficient associated with the vegetation type, for which Vargas-Luna et al. (2015) suggest using the value of 1, corresponding to rigid cylinders; n = vegetation density (m^{-1}), being $n = mD$, where m = number of cylinders per unit area (m^{-2}), D = cylinder diameter (m); and h_v = vegetation height (m).

The following simulations are performed:

- Preruns. Different model setups are run several times to check computational stability and to assess the time that is necessary to achieve morphodynamic equilibrium: T years.
- Calibration. Starting from a rectangular channel with the bank alignment and boundary conditions of 1800 AD, the model simulates the 2D development of the river bed topography for T years. The results are then compared to the measured 1800 AD bed topography. The value of unvegetated-bed Chézy coefficient is the one previously derived by Arboleda et al. (2010). The calibration parameter in this study is A_{sh} [Eq. (4)].
- Validation. Starting from the measured bed topography of 1800 AD, the model simulates the river bed evolution for 42 years. The results are then compared to the reconstructed bed topography of 1842 AD.
- Simulation scenarios. Starting with the bed topography of 1842 AD, the model is run for T years. *Base-case scenario:* this is without any interventions. *Wall scenarios W1 and W2*: the wall starts either upstream or downstream of point bar I top, and the river is subdivided in two equally-wide parallel channels. *Wall scenario W3*: the navigation channel width is 260 m, and the wall starts upstream of the bar top. *Groyne scenario G1*: the channel width is the current one (260 m), and the groynes have the general characteristic of the ones that are currently present in the Waal River (Yossef 2005), i.e., a length (protruding transversally to the flow) of 70 m, on average; a crest level equal to the river bank level; and a groyne field length (distance between two subsequent groynes) of 200 m. *Groyne scenario G2*: the channel width between groyne heads is equal to half of the historical Waal River width (200 m). In this case, the groyne length is 100 m on average, whereas the other groyne characteristics are the same as in scenario G1. In both scenarios, the channel alignment does not coincide with the present one, which has been straightened. Channel straightening would be an additional intervention leading to river adjustment, and for this, it is not considered in this study.

To compare the navigability and the high flow conveyance of the river in the different scenarios, the models are used again (this time with a fixed bed) to simulate the hydraulic conditions at selected values of the discharge (hydraulic models) (Castro-Bolinaga and Diplas 2014). The fixed-bed topographies are the final equilibrium ones resulting from the application of the morphodynamic model. For the Waal River, the discharge $Q_{\text{low}} = 680$ m^3/s is currently

used as the lowest value for which it is necessary to guarantee a minimum navigation depth of 2.80 m for a channel width of 150 m. The discharge of $Q_{design} = 10{,}600$ m^3/s is strongly recommended for the design of flood protection works. Another important reference discharge corresponds to the 1995 flood: 8,000 m^3/s (M. Schoor, personal communication, 2009–2018). These are the discharges considered in the hydraulic computations. The flow conveyance of the river is inferred by comparison of computed water levels at the same high discharge. Lower water levels indicate increased river conveyance whereas higher levels indicate decreased conveyance. The water levels are computed at a specific reference cross-section in the middle of the model domain.

Numerical Model Setup

The modeled river reach is about 12 km long and 1 km wide on average, with the width of the main channel (the historical Waal River) being approximately 400 m. The curvilinear grid follows the alignment of the historical channel with the embankments being used as land boundaries, with grid-cells of 40×20 m in the channel and 40×40 m in the floodplains. This configuration allows having a sufficient amount of data points along the cross section with a reasonable computational time. The morphological computations are not accelerated (Carraro et al. 2018).

For the calibration run, the initial main channel bed and the floodplains are horizontal in the transverse direction but sloping in the longitudinal direction, with slope $i_0 = 1 \times 10^{-4}$ and the floodplains being 5.5 m higher than the channel bed. For the validation run, the initial bed topography is the one derived from the 1800 map (Fig. 3). For the model simulations, the initial bed topography is the one derived from the 1842 map (Fig. 3).

The upstream hydraulic boundary condition is flow discharge. A representative yearly hydrograph [Fig. 4(b)] is derived from the mean duration curve of the period 1790–1810 [Fig. 4(a)], obtained from the data provided by Arboleda et al. (2010). The total volume of transported sediment computed using the representative yearly hydrograph [Fig. 4(b)] remains unchanged compared to the one obtained using the mean yearly duration curve [dotted red line in Fig. 4(a)]. The bed material, which is assumed uniform, has a diameter of 900 μm.

The representative yearly hydrograph is repeated every year for the entire duration of the computational period. The approach minimizes the problems related to model instability because it decreases the sudden inflow changes that are present in the reconstructed daily discharge time series while maintaining the same yearly sediment transport rates and almost the same yearly discharge distribution. The same approach has been already successfully used for long term morphological simulations by, for instance, Yossef et al. (2008). The downstream hydraulic boundary condition is a flow-dependent water level. In this study, the water level at the end of the model domain is assumed to coincide to the one corresponding to uniform flow.

The upstream boundary condition for the sediment component is a balanced sediment transport (recirculation: input = output). The downstream boundary condition is given by the free sediment transport condition, which allows undisturbed bed level changes up to the end of the model domain. The bed-load transport rate is computed with the Engelund and Hansen (1967) formula, valid for sand-bed rivers. The unvegetated bed roughness is represented by a constant Chézy coefficient, whereas the value of the Chézy coefficient of vegetated areas is computed by applying Eq. (5).

The distribution of floodplain vegetation cover is derived from the reconstructed ecotope maps of 1830 AD provided by Maas et al. (1997) (Fig. 5), and the vegetation parameters used in the model are the ones suggested by van Velzen et al. (2003) (Table 1). The computations are carried out, assuming that floodplain vegetation has not changed much in the 50 years covered by the simulations. The historical Waal River characteristics at an average discharge are listed in Table 2.

Results

Preruns

The results of the preruns show that a time step of 30 s ensures numerical stability and that after 50 years, the system reaches a state of morphodynamic equilibrium in which the longitudinal slope remains constant and cross-sectional changes of bed elevation are negligible ($T = 50$ years). The computational time of a 50-year simulation is 5–6 days.

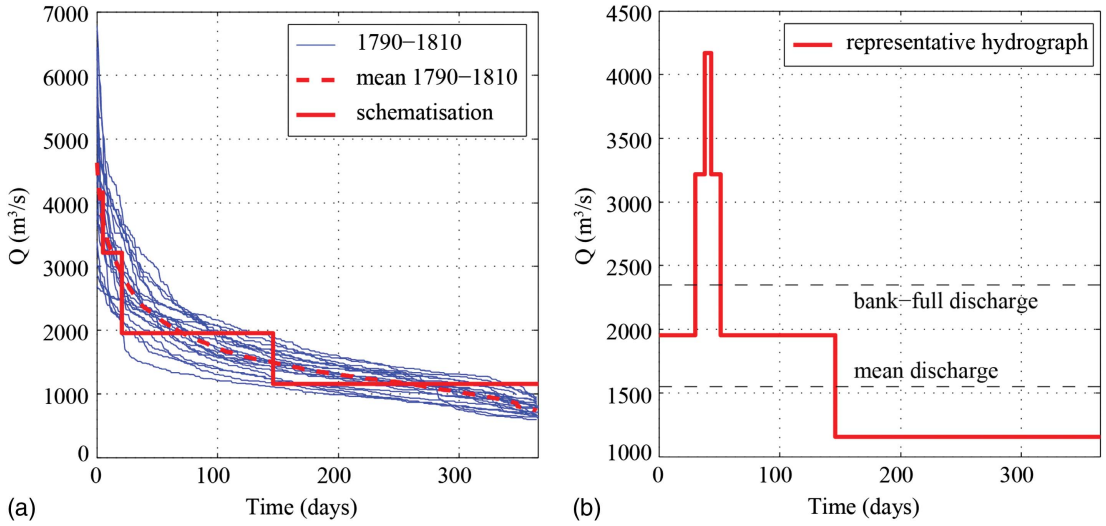

Fig. 4. (a) Annual duration curves based on daily discharge time series, mean duration curve, and schematized duration curve of the period 1790–1810; and (b) representative daily discharge hydrograph used in this study.

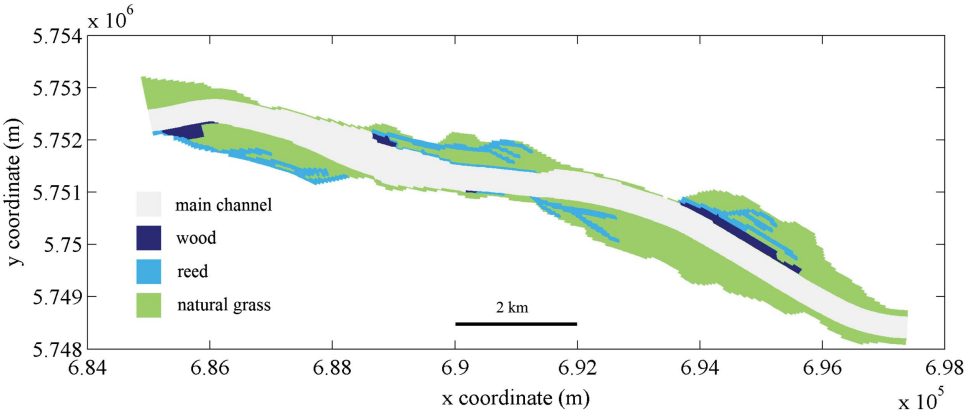

Fig. 5. Spatially varying vegetation cover in 1830 AD according to historical ecotope maps of Maas et al. (1997). Coordinates are in the Universal Transverse Mercator system.

Table 1. Selected vegetation types from typical floodplain vegetation according to van Velzen et al. (2003)

Vegetation type	h_v (m)	n (m^{-1})	C_D
Natural grass	0.1	21.6	1
Reed	2.5	0.6624	1
Wood	10	0.042	1

Note: The value of C_D, the drag coefficient, is imposed equal to 1, following the suggestion of Vargas-Luna et al. (2015).

Table 2. Reach-scale characteristics of the Waal River at average discharge in 1800 AD and sources

Parameters	Notation	Unit	Value	Source
River width	B_0	m	400	Maas et al. (1997)
Normal depth	h	m	6.0	Maas et al. (1997)
Longitudinal bed slope	i	—	10^{-4}	Maas et al. (1997)
Chézy coefficient	C	$m^{1/2}/s$	50	Arboleda et al. (2010)
Froude number	F	—	0.160	This study
Shields parameter	θ	—	0.026	This study
Width-to-depth ratio	B/h	—	30–70	This study

Model Calibration and Validation

Fig. 6 shows the results of model calibration. The computed bed topography presents three alternate bars in the main channel [Fig. 6(b)]. These bars are present and have a similar size in the reconstructed bed topography [Fig. 6(a)]. Fig. 6(c) shows both the reconstructed cross-section A-A and the computed one for different values of the calibration parameter. The best result is obtained for $A_{sh} = 0.4$. The results confirm what was reported by Le et al. (2018a): the larger A_{sh} (smaller bed slope effects) leads to larger bar amplitudes, shorter bar wavelengths, and smaller longitudinal slopes. The value of $A_{sh} = 0.4$ results in the longitudinal slope $i_{1800} = 1.03 \times 10^{-4}$, which is equal to the reconstructed longitudinal bed slope.

The calibrated model is then validated on its ability to reproduce the reconstructed bed topography of 1842 AD starting from the reconstructed bed topography of 1800 AD. Fig. 7 shows the results of the model validation. The model reproduces the chute cutoff that occurred in the period 1800–1842, resulting in the formation of a middle bar [Fig. 7(b)], which is similar to the one that can be observed from the reconstructed bed topography of 1842 [Fig. 7(a)]. Computed and reconstructed bars have similar lengths, but the model tends to underestimate the chute cutoff channel depth [Fig. 7(c)]. The computed longitudinal bed slope is $i_{1842} = 1.03 \times 10^{-4}$, which equals the reconstructed one. The satisfactory results of validation allow trusting the model in its ability to reproduce realistic bed topographies in the study area.

Long-Term Morphological Developments

The starting condition of all scenarios is the reconstructed bed topography of 1842 AD, improved by integrating the measured cross-sections with the computed bed topography. The computations, covering the period of 50 years, produce the hypothetical equilibrium situation at the end of 1892 AD, which is obtained without any morphological acceleration. The discharge hydrograph used as an upstream boundary condition is the schematized yearly hydrograph 1790–1810 (Fig. 4).

The computed 1892 bed topography of the base-case scenario (Fig. 8) shows that the channel to the left of the middle bar tends to silt up, whereas the channel to the right has become the main stream. Because the model does not simulate bank erosion, the main stream narrows to 120 m. This result is supported by the later performed historical works, belonging to the *Normalization* program (Fig. 1). Due to its decreased size since 1872, the left channel was finally abandoned after the construction of groynes (in 1888 and 1890, see Fig. 1), whereas the right channel was artificially straightened and enlarged to 310 m by removing the middle bar. The averaged longitudinal bed slope at the end of the 50-year evolution is the same as the 1842 slope: $i_{\text{untrain}} = 1.03 \times 10^{-4}$.

The results of the two wall scenarios in which the parallel channels have a width of 200 m are shown in Fig. 9. The final system always presents a deeper and a shallower channel. If the training wall starts upstream of point bar I top, the left channel gradually silts up and the right channel deepens [Fig. 9(a)]. Instead, if the wall starts downstream of the same point bar top, the left channel deepens, and the right channel silts up [Fig. 9(b)]. These results confirm the experimental and computational findings of Le et al. (2018a, b). Compared to the base-case scenario, the averaged bed level of the navigation channel lowers by either 3.57 m or 3.66 m for the starting locations at the upstream or downstream of point bar I top, respectively. The bed slopes become milder than in the base-case scenario: 0.91×10^{-4} and 0.89×10^{-4}, respectively, compared to $i_{\text{untrain}} = 1.03 \times 10^{-4}$. The bed level of the ecological channel raises by either 3.38 m or 3.76 m, respectively, and its bed slope becomes steeper than the one of the untrained river (base-case scenario): 3.80×10^{-4} and 3.77×10^{-4}, respectively.

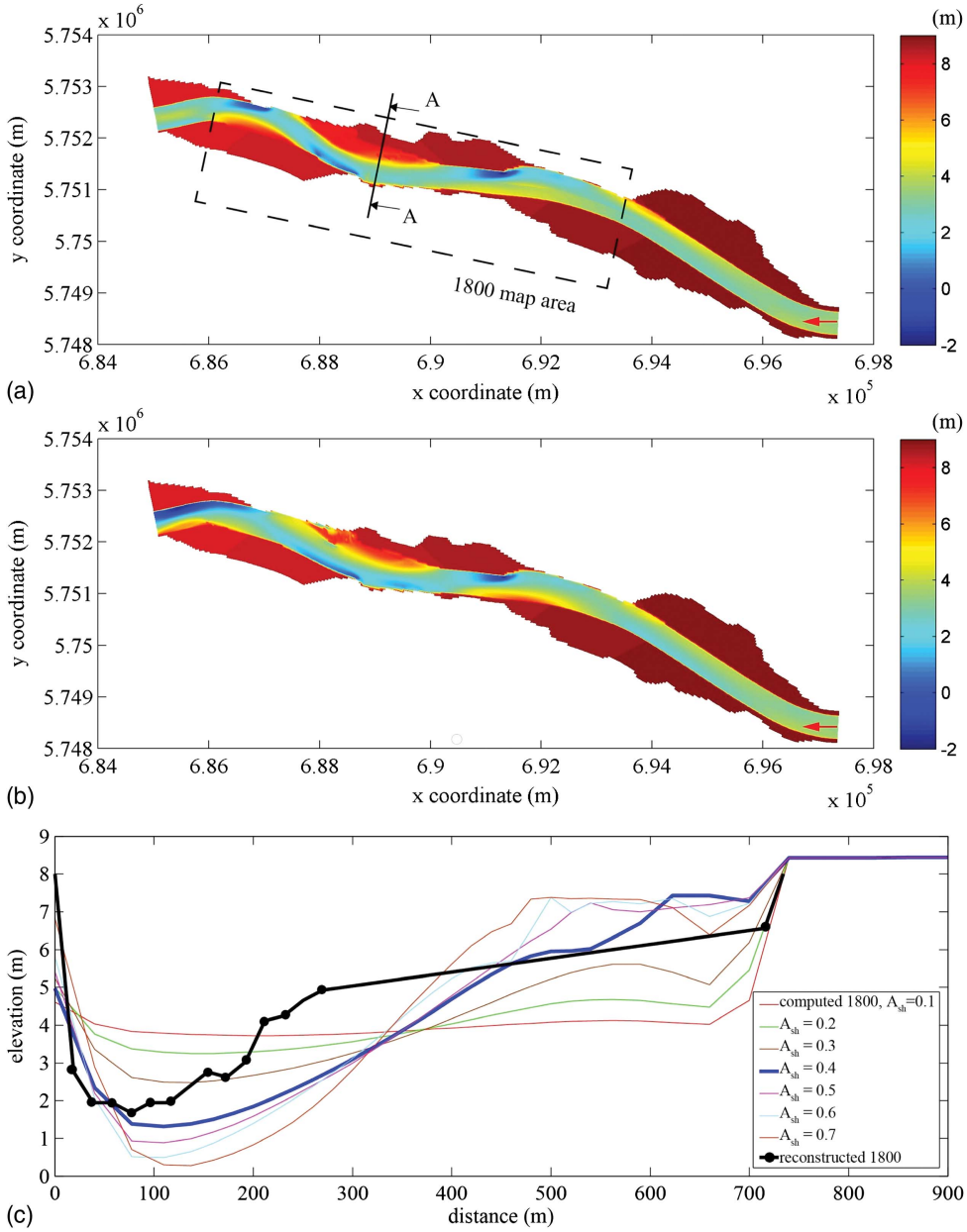

Fig. 6. Results of model calibration: (a) reconstructed riverbed topography in 1800 AD and localization of Section A-A; (b) computed riverbed topography in 1800 AD with $A_{sh} = 0.4$ (coordinates are in the Universal Transverse Mercator system); and (c) computed and reconstructed bed levels in 1800 AD at cross-section A-A. Values are relative to the current sea reference level (best fit with $A_{sh} = 0.4$).

In the two groyne scenarios, the channel between groyne heads has either the width of the current Waal River (260 m) or of 200 m. Fig. 10 shows the computed bed topographies. In this figure, the river channel has clearly deepened, as described by Suzuki et al. (1987) and Spannring (1999). Compared to the untrained river scenario (base-case), the averaged bed level lowers by either 2.33 or 4.04 m for the river width of 260 or 200 m, respectively. The bed slope becomes milder: 0.93×10^{-4} and 0.87×10^{-4}, respectively, compared to $i_{\text{untrain}} = 1.03 \times 10^{-4}$. The results agree with the general trends that can be expected after river narrowing (Duró et al. 2015).

Channel Incision

Jansen et al. (1979) and Duró et al. (2015) show that channel narrowing inevitably leads to river incision in the narrowed reach and upstream. In the narrowed reach, incision is caused by channel deepening and by a longitudinal bed slope reduction. A longitudinal slope reduction lowers the bed and water levels at the upper end of the narrowed reach. This triggers an erosion process propagating upstream in which the final bed level lowering is theoretically equal to the slope reduction multiplied by the length of the narrowed reach. This means that the training setup that results in the smallest longitudinal slope has the highest effect upstream.

Table 3 lists the values of average channel deepening and final equilibrium longitudinal slopes of all considered scenarios. In general, the navigation channel obtained with a longitudinal wall presents less deepening compared to an equally-wide navigation channel obtained with groynes. However, the difference appears negligible for the width of 260 m. Starting the wall just upstream of the point bar top slightly reduces the averaged riverbed lowering compared to starting the wall downstream.

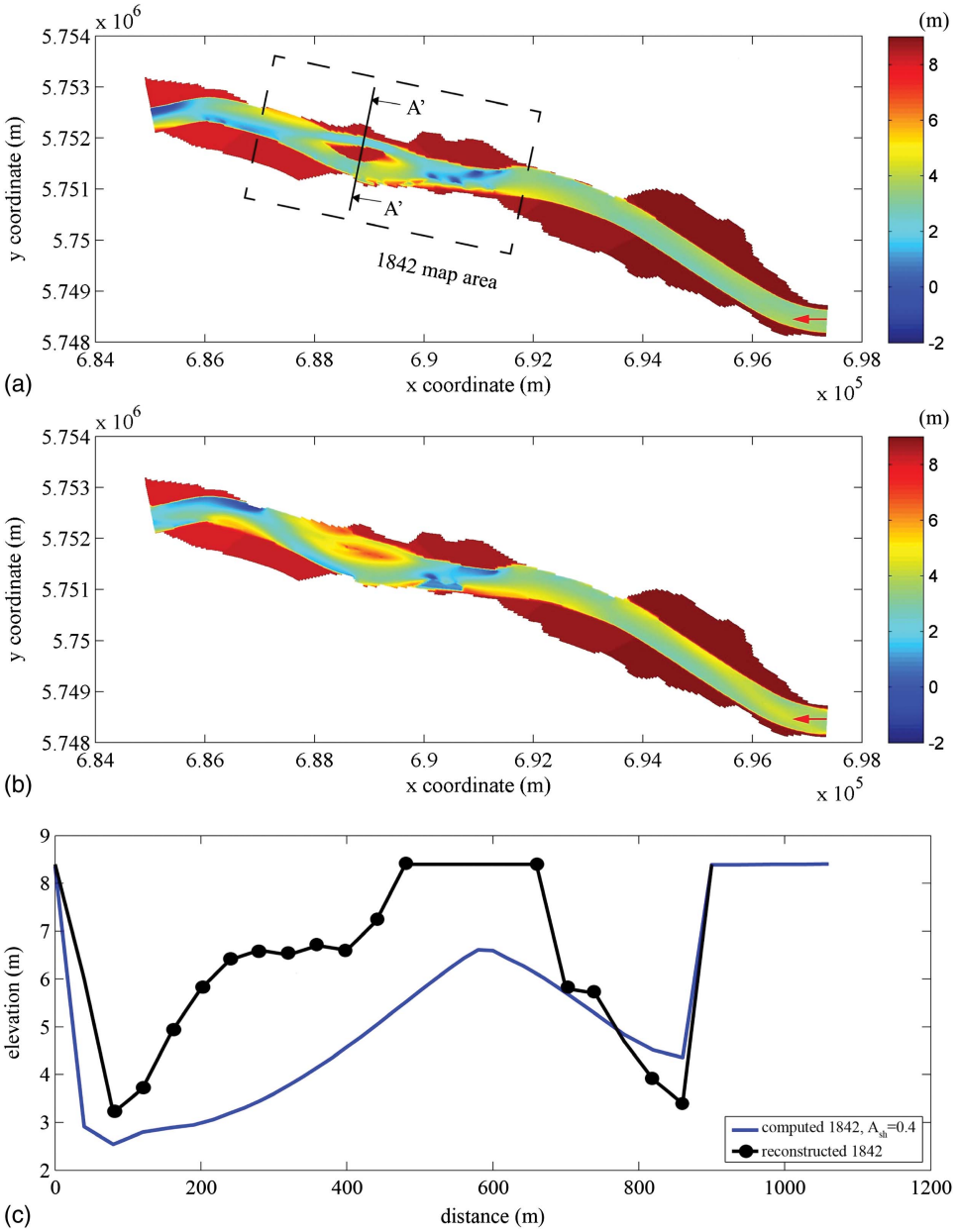

Fig. 7. Results of model validation: (a) reconstructed riverbed topography in 1842 AD and localization of Section A'-A'; (b) computed riverbed topography in 1842 AD with $A_{sh} = 0.4$ (coordinates are in the Universal Transverse Mercator system); and (c) computed and reconstructed bed levels in 1842 AD at cross-section A'-A'. Values are relative to the current sea reference level.

The results show that the groyne scenario with a river width of 200 m presents the largest impact on the longitudinal slope, whereas the wall scenario with a navigation channel width of 260 m presents the smallest one. Even if the differences appear small, these might result in important differences in upstream river incision if the trained reach has a length of the order of 100 km, as it is for the River Waal in the Netherlands.

River Navigability

To check river navigability, the models are used to assess the water depths at the prescribed minimum discharge considering the computed bed topographies of 1892 AD (hydraulic models).

The results, shown in Fig. 11(a), indicate that in the base-case scenario, the river fulfills the criterion for navigation depth only in the right channel around the middle bar where the width is 120 m, which is smaller than the minimum requirement. In all the groyne scenarios [Figs. 11(d and e)], and in the wall scenarios subdividing the river in two 200 m-wide parallel channels [Figs. 11(b and c)], the minimum water depth of 2.8 m is exceeded everywhere. The results of the wall scenario with a navigation channel of 260 m are shown in Fig. 12. In this case, some bars form in local channel expansion areas, where the flow presents larger width-to-depth ratios. As a result, the navigation channel would need a flattening of bar tops or local width adjustments to maintain a depth of 2.8 m over the entire width. The formation of bars leading to local water depths smaller than 2.8 m does not occur in the groyne scenario with the same width [Fig. 11(d)] because of the absence of channel expansion areas. Nevertheless, bar tops flattening is regularly carried out in the current Waal River having the same width of 260 m (M. Schoor, personal communication, 2009–2018).

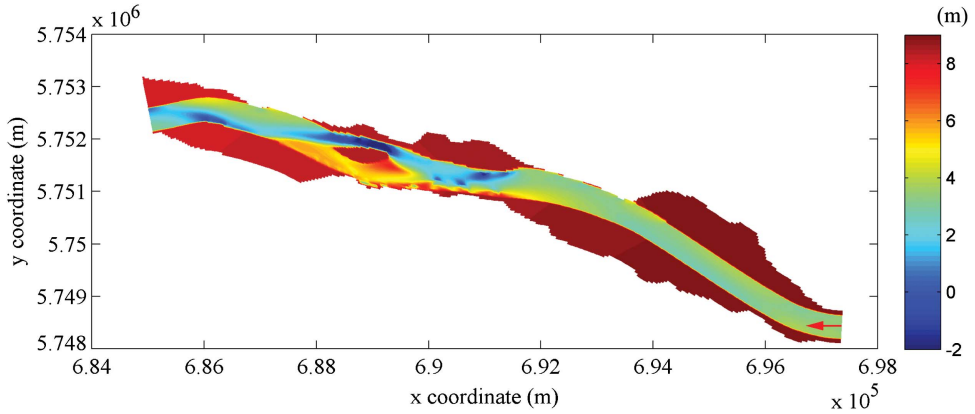

Fig. 8. Base-case scenario (untrained river): computed bed topography at the end of 1892 AD. Coordinates are in the Universal Transverse Mercator system. Values are relative to the current sea reference level.

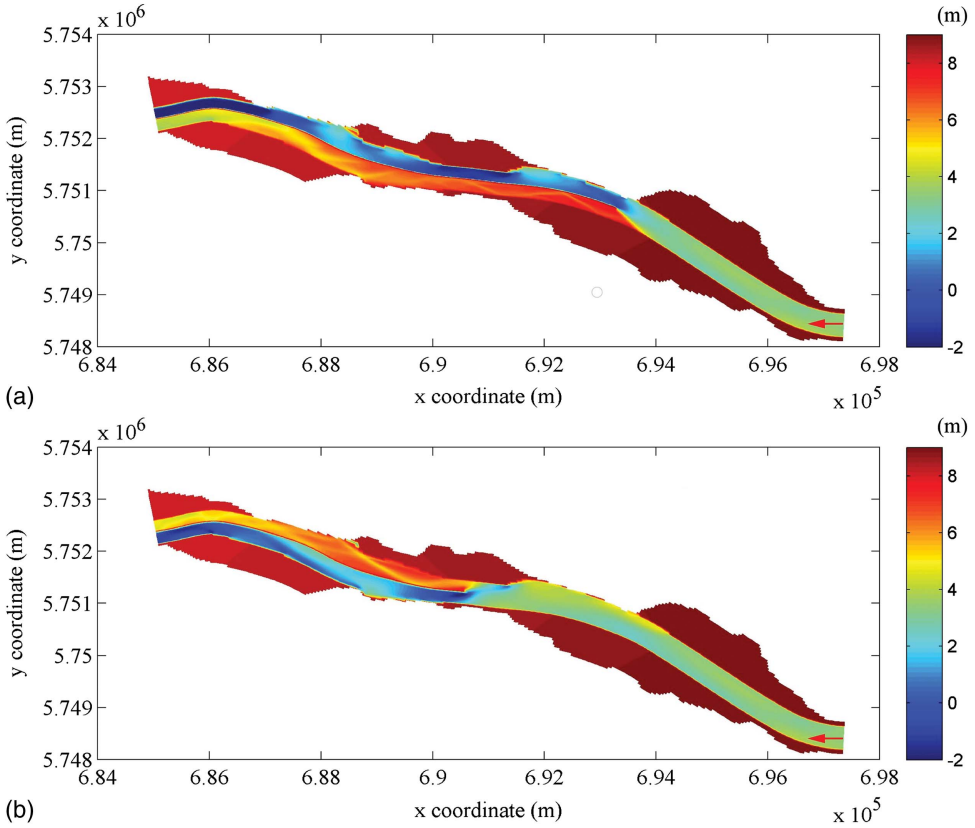

Fig. 9. Wall scenarios. Computed bed topography at the end of 1892 AD (values are relative to the current sea reference level): (a) scenario in which the longitudinal training wall starts upstream of point bar I top; and (b) scenario in which the longitudinal training wall starts downstream of point bar I top. The location of point bar I is indicated in Fig. 3(a). Coordinates are in the Universal Transverse Mercator system.

High Flow Conveyance

The hydraulic models are also used to compute the water levels at high flows. The effects of river training on water levels are represented in this study by ΔZ_{water}. This is the difference between the average water level of the considered training scenario and the one of the base-case scenario at Cross-Section A'-A', assumed as representative of the study river reach [Fig. 7(a)]. If ΔZ_{water} is negative, the training method results in lower water levels, which indicates increased high flow conveyance of the river and vice versa if it is positive. The computed water levels at Cross-Section A'-A' are listed in Table 4.

The results show that the longitudinal training wall increases the high flow conveyance even compared to the untrained river. This is due to navigation channel deepening. The most appropriate starting location of the wall is upstream of the point bar top. Instead, training by means of a series of groynes decreases the high flow conveyance of the river, potentially creating problems during floods.

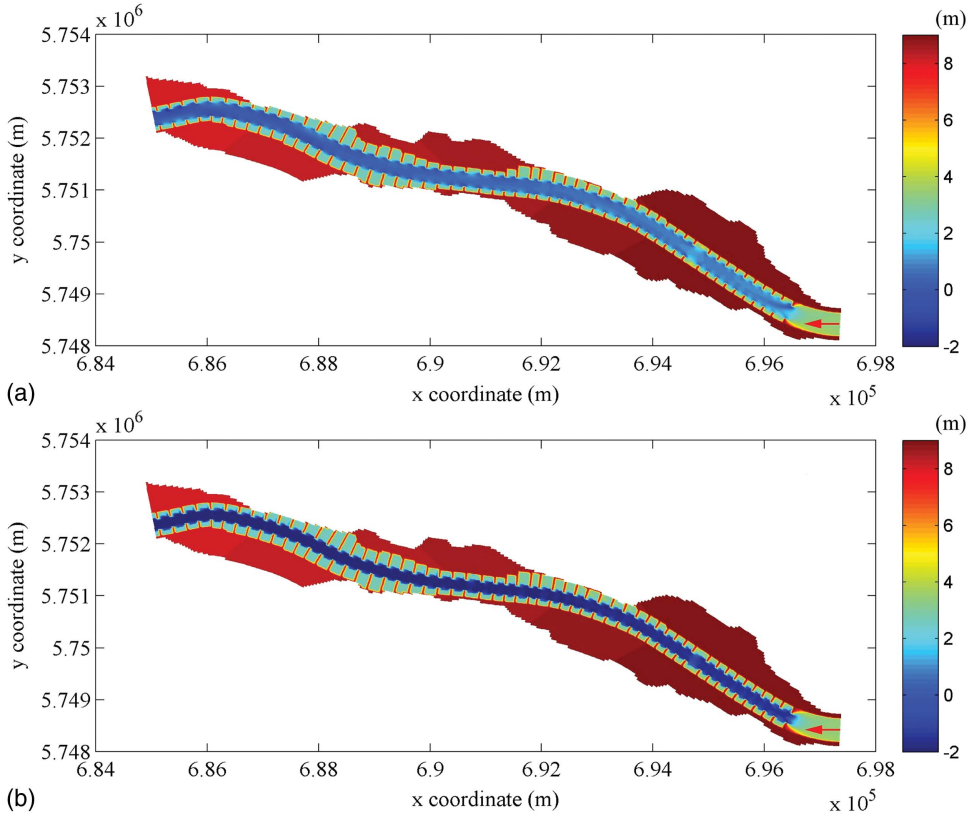

Fig. 10. Groyne scenarios. Computed bed topography at the end of 1892 AD (values are relative to the current sea reference level): (a) scenario with river width 260 m; and (b) scenario with river width 200 m. Coordinates are in the Universal Transverse Mercator system.

Table 3. Longitudinal navigation channel slope at final equilibrium (1892 AD) and average navigation channel deepening with respect to the untrained river case

Scenario	Longitudinal bed slope	Averaged bed level with respect to base-case scenario (m)
(Base-case): untrained river	1.03×10^{-4}	0
Wall (W1): upstream, navigation channel width 200 m	0.91×10^{-4}	−3.57
Wall (W2): downstream, navigation channel width 200 m	0.89×10^{-4}	−3.66
Wall (W3): upstream, navigation channel width 260 m	0.98×10^{-4}	−2.30
Groyne (G1): river width 260 m	0.93×10^{-4}	−2.33
Groyne (G2): river width 200 m	0.87×10^{-4}	−4.04

Discussion

The results presented in this study are affected by uncertainties. However, the computed values are only used to compare scenarios, and for this reason, the approach can be still considered appropriate, even if some aspects can be more relevant in one scenario rather than in another one. For more realistic results, a few aspects should be considered.

The investigation is based on the use of 2DH models, which cannot correctly simulate the flow that overtops the wall and the groynes at high-discharge conditions. Water levels at flows above bankfull are strongly affected by the resistance of groynes and the wall (Huthoff et al. 2013). There is still debate about whether the groyne resistance is properly calculated by 2DH models because experimental investigations showed complex processes around groynes and in their fields (Uijttewaal 2005; Yossef and de Vriend 2011). In any case, the groynes and the flow around and above them are not well resolved. This might lead to important errors on water levels estimates. Similarly, errors can be caused by an inaccurate representation of the flow along and above the wall. This means that the results regarding the flow conveyance of the river are not conclusive and further investigation is needed. With particular regard to the wall scenarios, the models also do not reproduce well the working of the system navigation-ecological channel when important flow exchanges between the two channels can be expected. To improve the results, a three-dimensional model with a detached eddy simulation (DES) is needed. Such a model would also allow studying the effects of suspended solids, which are not taken into account in the present study. A deposition of fine material might accelerate sedimentation in the ecological channel and increase its final bed level rise.

Another aspect that has not been investigated in this study is bank erosion. Whereas it is clear that bank protection is needed along the navigation channel, the results indicate that the ecological channel can maintain a natural bank. However, bank erosion can occur also along the ecological channel, in particular during high

flow conditions, when ship waves can reach the unprotected bank (Rutherfurd et al. 2007). Preliminary data collected in the framework of the project *Waalsamen* along the ecological channels behind the three pilot longitudinal dams built in the Waal River (Fig. 2) indicate the occurrence of bank erosion during high flow conditions (M. Schoor, personal communication, 2009–2018). This means that future research should also include bank processes.

The models simulate strongly schematized scenarios. For instance, the longitudinal wall is represented without any openings, i.e., without any water exchange between the two parallel channels. Due to this, the channels present different water levels. Moreover, the model domain is a relatively short river reach. The results are thus affected by the boundary conditions.

Topographical information of the floodplains in the nineteenth century is not available, so floodplains were schematized as horizontal surfaces with a longitudinal slope $i_0 = 1 \times 10^{-4}$ (Fig. 5). This approximation needs further improvements because the present floodplain levels of the Waal floodplains can vary by 3–4 m (Middelkoop and Asselman 1998).

Finally, the investigation does not consider colonization and growth of vegetation in the ecological channel during low-flow conditions. This, by increasing the hydraulic resistance, might have the following effects: rise of water levels at high flow conditions and increased sedimentation in the ecological channel leading to its total closure. Future investigations should consider these aspects and investigate the effects of different vegetation management strategies, as well as dredging strategies.

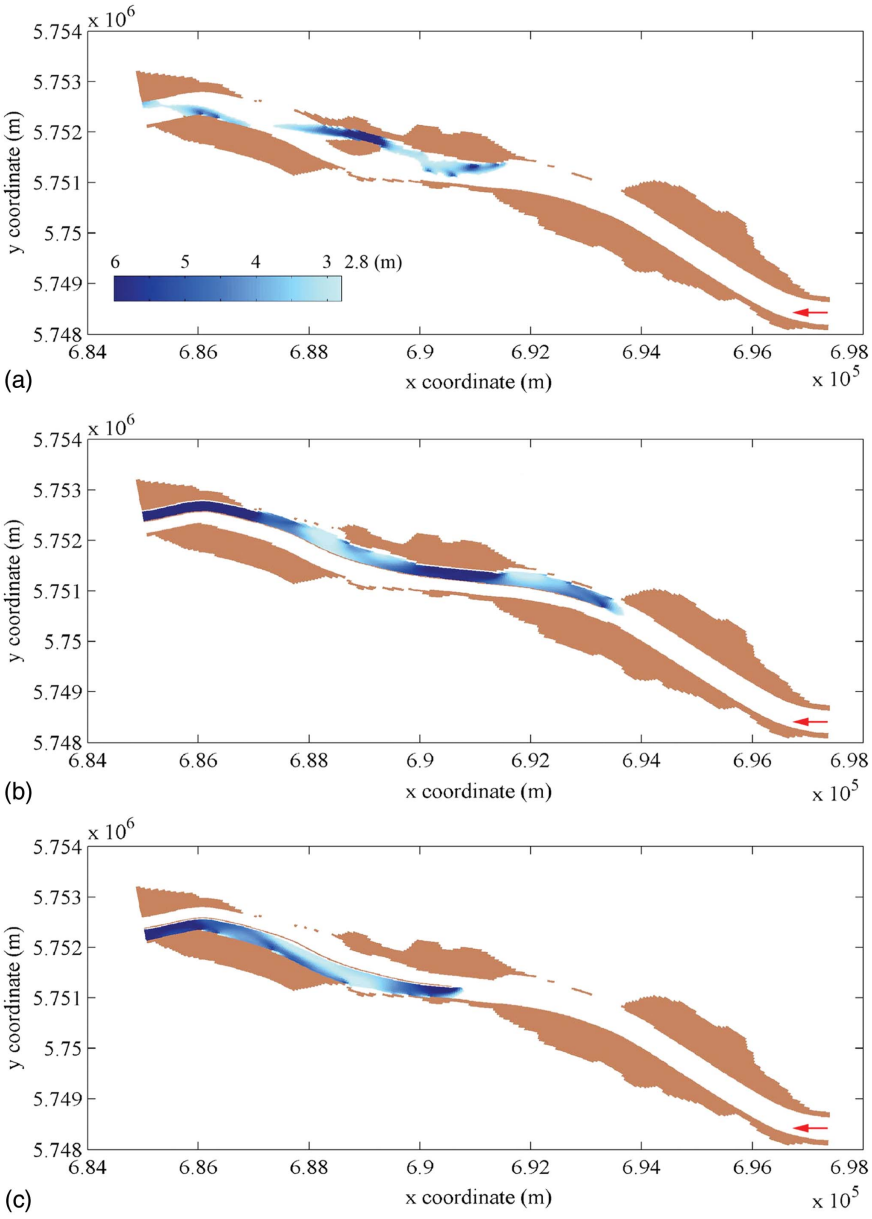

Fig. 11. Water depth distribution at low-flow ($Q_{low} = 680$ m^3/s). Flood plains and training structures are colored brown. Gray areas in the water body indicate local water depth less than 2.8 m: (a) base-case scenario (average water depth: 1.86 m); (b) wall scenario, with wall starting upstream of point bar I top and navigation channel width equal to 200 m (average water depth: 5.13 m); (c) wall scenario with wall starting downstream of point bar I top and navigation channel width equal to 200 m (average water depth: 5.16 m); (d) groyne scenario with river-flow width of 260 m (average water depth: 3.99 m); and (e) groyne scenario with river-flow width of 200 m (average water depth: 5.17 m). The location of point bar I is indicated in Fig. 3(a). Coordinates are in the Universal Transverse Mercator system.

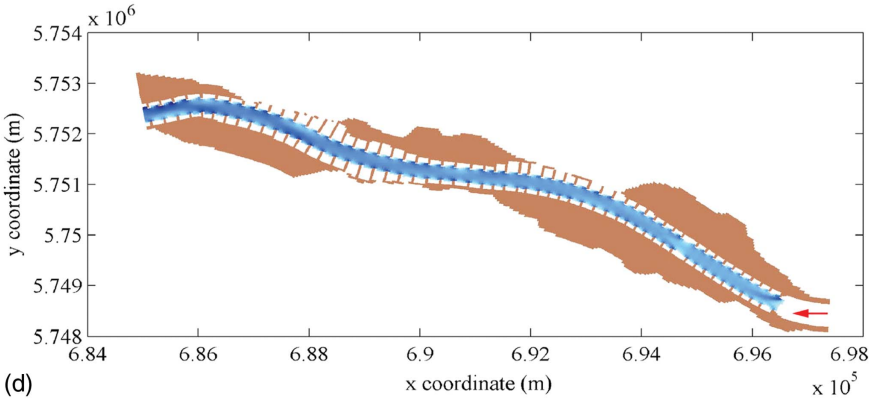

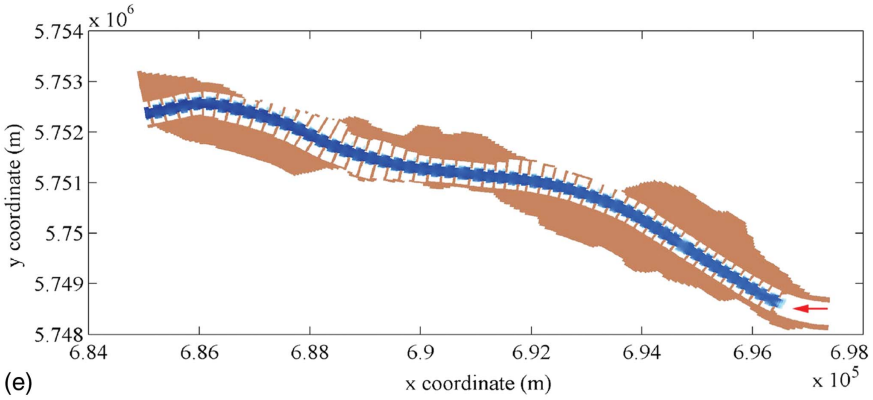

Fig. 11. (*Continued.*)

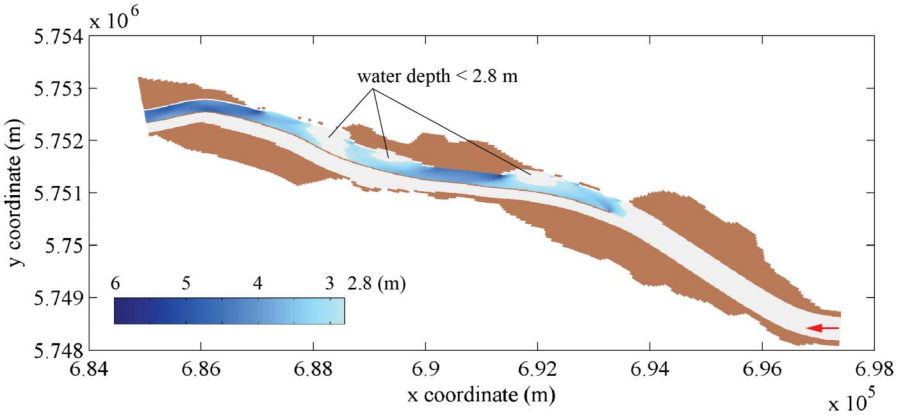

Fig. 12. Water depth at $Q_{low} = 680$ m^3/s in W3 run. Flood plains and training structures are colored brown. Gray areas in the water body indicate a local water depth less than 2.8 m. Coordinates are in the Universal Transverse Mercator system.

Table 4. Average water levels at Cross-Section A'-A' in 1892 AD (computed equilibrium bed topographies)

	$Q_{history} = 8{,}000$ m^3/s		$Q_{design} = 10{,}600$ m^3/s	
Scenarios	Water level (m)	ΔZ_{water} (m)	Water level (m)	ΔZ_{water} (m)
(Base-case): untrained river	11.02	—	13.08	—
Wall (W1): upstream, navigation channel width 200 m	10.77	−0.25	12.95	−0.13
Wall (W2): downstream, navigation channel width 200 m	10.90	−0.12	13.06	−0.02
Wall (W3): upstream, navigation channel width 260 m	10.74	−0.28	12.91	−0.17
Groyne (G1): river width 260 m	11.12	+0.10	13.15	+0.07
Groyne (G2): river width 200 m	11.20	+0.18	13.20	+0.12

Table 5. Summary of advantages and disadvantages of river training with a longitudinal wall with respect to groynes in the Waal River

Navigation channel width	Navigability	High flow conveyance	Incision	Potential river ecology
W1 (200 m)	0	++	+	++
W2 (200 m)	0	++	+	++
W3 (260 m)	—[a]	++	+	++

[a]Requires flattening of bar tops or removal of local width expansions for low-flow navigability.

Conclusions and Recommendations

This work addresses the long-term developments of the historical Waal River with different training techniques to assess whether a longitudinal training wall subdividing the river in two parallel channels would have resulted in more favorable conditions than the current groyne fields. The morphological evolution and the hydraulic conditions have been investigated by means of a 2DH numerical model developed using the Delft3D code. Several training scenarios are considered. The analysis is based on the comparison between river morphology, navigability level, and high flow conveyance at equilibrium, considering also the *natural* untrained river case.

The model is calibrated and validated on the reconstructed bed topographies of 1800 and 1842 AD, respectively. The results show that the historical morphological developments are reproduced in a satisfactory way and that the model can then be used for these types of investigations.

The results of the numerical simulations covering 50 years, starting from the riverbed topography of 1842 AD, show that separating the Waal River by a longitudinal training wall always leads to the formation of one deeper and one shallower channel. The starting position of the wall with respect to a steady bar determines which channel becomes the deeper navigation channel and which one becomes the shallower ecological channel. This agrees with the findings of Le et al. (2018a, b). The reach-scale characteristics of the navigation channels obtained with different starting positions of the longitudinal wall are similar. Starting the wall just upstream of a point bar top slightly reduces river incision, which arises from the local bed level lowering and longitudinal slope reduction (Jansen et al. 1979; Duró et al. 2015). A smaller reduction of the longitudinal bed slope in the narrowed reach is always desirable because upstream river incision might become significant if the narrowed reach is very long (hundreds of kilometers). In general, the deepening of the navigation channel shows the need of protecting its bank, whereas bank protection might not be necessary for the ecological channel.

For the same navigation channel width, the results of the computations show that the implementation of a longitudinal wall instead of a series of groynes would not result in different levels of navigability. In all considered cases, the minimum criteria for navigation are satisfied. These criteria are not met in the untrained river case, showing that the current navigability criterion can only be achieved in the Waal River by means of river training, which is in fact what has happened in reality. The results show also that a longitudinal wall is much preferable when considering the high-flow conveyance of the river. Also, with respect to this criterion, the most appropriate starting location of the wall is just upstream of a point bar top. The presence of a shallow channel with a natural bank is another reason to prefer the longitudinal wall to the groynes because this potentially increases the river ecological value (Radspinner et al. 2010; Collas et al. 2018).

Table 5 summaries the advantages and disadvantages of longitudinal walls. Single plus indicates slight improvement with respect to the groyne scenario having the same navigation channel width. Double plus indicates improvement with respect to all considered groyne scenarios. A zero value indicates a neutral effect and a minus indicates a negative effect compared to groyne scenarios.

The results of this study suggest that a longitudinal training wall might be an appropriate intervention to train wide low-land rivers as water ways. It is advisable to carefully select the location of the upstream end of the wall if the channel bed presents steady bars or point bars. In this case, the most favorable location to start the wall is just upstream of a steady bar or point bar top. Placing the wall in the middle of the channel maximizes system stability. The bank of the navigation channel should be protected and properly aligned, whereas the study does not indicate the need for ecological-channel bank protection.

Data Availability Statement

The models developed during the study are available from the corresponding author by request. Data were provided by a third party. Direct requests for these materials may be made to the provider as indicated in the Acknowledgments.

Acknowledgments

This work is sponsored by the Vietnam International Education Development (VIED), project 911. The authors wish to acknowledge the useful comments provided by Wim S. J. Uijttewaal and Erik Mosselman and to thank Rijkswaterstaat—Ministry of Infrastructure and Water Management, the Netherlands, for providing important data and information on the Waal River. This research has benefited from cooperation within the network of the Netherlands Centre for River Studies.

References

Arboleda, A. M., A. Crosato, and H. Middelkoop. 2010. "Reconstructing the early 19th-century Waal River by means of a 2D physics-based numerical model." *Hydrol. Processes.* 24 (25): 3661–3675. https://doi.org/10.1002/hyp.7804.

Baptist, M. J., L. V. van Den Bosch, J. T. Dijkstra, and S. Kapinga. 2003. "Modelling the effects of vegetation on flow and morphology in rivers." *Large Rivers* 15 (1–4): 339–357. https://doi.org/10.1127/lr/15/2003/339.

Bertoldi, W., and M. Tubino. 2007. "River bifurcations: Experimental observations on equilibrium configurations." *Water Resour. Res.* 43 (10): W10437. https://doi.org/10.1029/2007WR005907.

Carraro, F., D. Vanzo, V. Cale, A. Valiania, and A. Siviglia. 2018. "Mathematical study of linear morphodynamic acceleration and derivation of the MASSPEED approach." *Adv. Water Resour.* 117 (Jul): 40–52. https://doi.org/10.1016/j.advwatres.2018.05.002.

Castro-Bolinaga, C. F., and P. Diplas. 2014. "Hydraulic modeling of extreme hydrologic events: Case study in southern Virginia." *J. Hydraul. Eng.* 140 (12): 05014007. https://doi.org/10.1061/(ASCE)HY.1943-7900.0000927.

Collas, F. P. L., A. D. Buijse, L. van den Heuvel, N. van Kessel, M. M. Schoor, H. Eerden, and R. S. E. W. Leuven. 2018. "Longitudinal training dams mitigate effects of shipping on environmental conditions and fish density in the littoral zones of the river Rhine." *Sci. Total Environ.* 619–620 (Apr): 1183–1193. https://doi.org/10.1016/j.scitotenv.2017.10.299.

Deltares. 2014. "Simulation of multi-dimensional hydrodynamic flows and transport phenomena, including sediments." Accessed May 28, 2014.

https://oss.deltares.nl/documents/183920/185723/Delft3D-FLOW_User_Manual.pdf.
Duró, G., A. Crosato, and P. Tassi. 2015. "Numerical study on river bar response to spatial variations of channel width." *Adv. Water Resour.* 93 (Jul): 21–38. https://doi.org/10.1016/j.advwatres.2015.10.003.
Engelund, F., and E. Hansen. 1967. *A monograph on sediment transport in alluvial streams*. Copenhagen, Denmark: Danish Technical Press.
Frings, R. M., B. M. Berbee, G. Erkens, M. G. Kleinhans, and M. J. P. Gouw. 2009. "Human-induced changes in bed shear stress and bed grain size in the River Waal (the Netherlands) during the past 900 years." *Earth Surf. Processes Landforms* 34 (4): 503–514. https://doi.org/10.1002/esp.1746.
Frings, R. M., and M. G. Kleinhans. 2008. "Complex variations in sediment transport at three large river bifurcations during discharge waves in the river Rhine." *Sedimentology* 55 (5): 1145–1171. https://doi.org/10.1111/j.1365-3091.2007.00940.x.
Henket, N. H., C. M. Schols, and J. M. Telders. 1885–1890. *Waterbouwkunde (4 parts in 8 books)*. [In Dutch.] s-Gravenhage: De Gebroeders van Cleef.
Huthoff, F., N. Pinter, and J. W. F. Remo. 2013. "Theoretical analysis of wing dike impact on river flood stages." *J. Hydraul. Eng.* 139 (5): 550–556. https://doi.org/10.1061/(ASCE)HY.1943-7900.0000698.
Jansen, P. P., L. van Bendegom, J. van den Berg, M. de Vries, and A. Zanen. 1979. *Principles of river engineering. The non-tidal alluvial river*. London: Pitman.
Kleinhans, M. G., H. R. A. Jagers, E. Mosselman, and C. J. Sloff. 2008. "Bifurcation dynamics and avulsion duration in meandering rivers by one-dimensional and three-dimensional models." *Water Resour. Res.* 44 (8): W08454. https://doi.org/10.1029/2007WR005912.
Koch, F. G., and C. Flokstra. 1981. "Bed level computations for curved alluvial channels." In Vol. 2 of *Proc., 19th Congress IAHR*, Delft, Netherlands: Delft Hydraulics Laboratory.
Le, T. B., A. Crosato, E. Mosselman, and W. S. J. Uijttewaal. 2018a. "On the stability of river bifurcations created by longitudinal training walls. Numerical investigation." *Adv. Water Resour.* 113 (Mar): 112–125. https://doi.org/10.1016/j.advwatres.2018.01.012.
Le, T. B., A. Crosato, and W. S. J. Uijttewaal. 2018b. "Long-term morphological developments of river channels separated by a longitudinal training wall." *Adv. Water Resour.* 113 (Mar): 73–85. https://doi.org/10.1016/j.advwatres.2018.01.007.
Maas, G. J., H. P. Wolfert, M. M. Schoor, and H. Middelkoop. 1997. *Classificatie van riviertrajecten en kansrijkdom voor ecotopen*. [In Dutch.] Rep. No. 552. Wageningen, Netherlands: DLOStaring Centrum.
McCoy, A., G. Constantinescu, and L. J. Weber. 2008. "Numerical investigation of flow hydrodynamics in a channel with a series of groynes." *J. Hydraul. Eng.* 134 (2): 157–172. https://doi.org/10.1061/(ASCE)0733-9429(2008)134:2(157).
Middelkoop, H. 1997. "Embanked floodplains in the Netherlands: Geomorphological evolution over various time scales." Ph.D. thesis, Faculty of Geographical Sciences, Univ. of Utrecht.
Middelkoop, H., and N. E. M. Asselman. 1998. "Spatial variability of floodplain sedimentation at the event scale in the Rhine-Meuse Delta, the Netherlands." *Earth Surf. Processes Landforms* 23 (6): 561–573. https://doi.org/10.1002/(SICI)1096-9837(199806)23:6<561::AID-ESP870>3.0.CO;2-5.
Mosselman, E., and T. B. Le. 2016. "Five common mistakes in fluvial morphodynamic modeling." *Adv. Water Resour.* 93 (Jul): 15–20. https://doi.org/10.1016/j.advwatres.2015.07.025.
Radspinner, R. R., P. Diplas, A. F. Lightbody, and F. Sotiropoulos. 2010. "River training and ecological enhancement potential using in-stream structures." *J. Hydraul. Eng.* 136 (12): 967–980. https://doi.org/10.1061/(ASCE)HY.1943-7900.0000260.
Rutherfurd, I., G. Vietz, J. Grove, and R. Lawrence. 2007. *Review of erosion control techniques on the river Murray between Hume Dam and Lake Mulwala*. Parkville, VIC, Australia: Univ. of Melbourne.
Schoor, M. M., H. P. Wolfert, G. J. Maas, H. Middelkoop, and J. P. Lambeek. 1999. "Potential for floodplain rehabilitation based on historical maps and present-day processes along the River Rhine, the Netherlands." In Vol. 163 of *Floodplains: Interdisciplinary approaches*, edited by S. B. Marriott and J. Alexander, 123–137. London: Geological Society.
Schuurman, F., W. A. Marra, and M. G. Kleinhans. 2013. "Physics-based modeling of large braided sand-bed rivers: Bar pattern formation, dynamics, and sensitivity." *J. Geophys. Res. Earth Surf.* 118 (4): 2509–2527. https://doi.org/10.1002/2013JF002896.
Sieben, J. 2009. "Sediment management in the Dutch Rhine branches." *Int. J. River Basin Manage.* 7 (1): 43–53. https://doi.org/10.1080/15715124.2009.9635369.
Spannring, M. 1999. "Degradation of the river bed after building of groynes." In *Proc., 28th IAHR Congress*, 1–7. Graz, Austria: International Association for Hydro-Environment Engineering and Research.
Struiksma, N., K. Olesen, C. Flokstra, and H. D. Vriend. 1985. "Bed deformation in curved alluvial channels." *J. Hydraul. Res.* 23 (1): 57–79. https://doi.org/10.1080/00221688509499377.
Suzuki, K., M. Michiue, and O. Hinokidani. 1987. "Local bed form around a series of spur-dikes in alluvial channels." In *Proc., 22nd Congress IAHR*, 316–321. Lausanne, Switzerland: International Association for Hydro-Environment Engineering and Research.
Talmon, A. M., N. Struiksma, and M. C. L. M. van Mierlo. 1995. "Laboratory measurements of the direction of sediment transport on transverse alluvial-bed slopes." *J. Hydraul. Res.* 33 (4): 495–517. https://doi.org/10.1080/00221689509498657.
Uijttewaal, W. S. J. 2005. "Effects of groyne layout on the flow in groyne fields: Laboratory experiments." *J. Hydraul. Eng.* 131 (9): 782–791. https://doi.org/10.1061/(ASCE)0733-9429(2005)131:9(782).
van Velzen, E. H., P. Jesse, P. Cornelissen, and H. Coops. 2003. *Stromingsweerstand vegetatie in uiterwaarden*. [In Dutch.] Technical Rep. No. 2003Ð028. Arnhem, Netherlands: Rijkswaterstaat, RIZA.
van Vuren, W. 2005. *Verdeling zomer-en winterhoogwaters voor de Rijntakken in de periode 1770–2004*. [In Dutch.] Memo WRR 2005-012. The Hague, Netherlands: Wetenschappelijke Raad Voor het Regeringsbeleid.
Vargas-Luna, A., A. Crosato, N. Anders, A. J. F. Hoitink, S. D. Keesstra, and W. S. J. Uijttewaal. 2018. "Morphodynamic effects of riparian vegetation growth after stream restoration." *Earth Surf. Processes Landforms* 43 (8): 1591–1607. https://doi.org/10.1002/esp.4338.
Vargas-Luna, A., A. Crosato, G. Calvani, and W. S. J. Uijttewaal. 2015. "Representing plants as rigid cylinders in experiments and models." *Adv. Water Resour.* 93 (Jul): 205–222. https://doi.org/10.1016/j.advwatres.2015.10.004.
Wijbenga, J. H. A., J. J. P. Lambeek, E. Mosselman, R. L. J. Nieuwkamer, and R. H. Passchier. 1993. *Toetsing uitgangspunten rivierdijkversterkingen; Deelrapport 2: Maatgevende belastingen*. [In Dutch.] Delft, Netherlands: Waterloopkundig Laboratorium and European-American Center for Policy Analysis.
Wijbenga, J. H. A., J. J. P. Lambeek, E. Mosselman, R. L. J. Nieuwkamer, and R. H. Passchier. 1994. "River flood protection in the Netherlands." In *Proc., Int. Conf. on River Flood Hydraulics*, editors W. R. White and J. Watts, 275–285. York, UK: Wiley.
Yossef, M. F. M. 2005. "Morphodynamics of rivers with groynes." Ph.D. thesis, Faculty of Civil Engineering and Geosciences, Delft Univ. of Technology.
Yossef, M. F. M., and H. J. de Vriend. 2011. "Flow details near river groynes: Experimental investigation." *J. Hydraul. Eng.* 137 (5): 504–516. https://doi.org/10.1061/(ASCE)HY.1943-7900.0000326.
Yossef, M. F. M., C. Stolker, S. Giri, A. Hauschild, and S. van Vuren. 2008. *Calibration of the multi-domain model*. Rep. No. Q4357.20. Delft, Netherlands: WL Delft Hydraulics.